Journal of Fluorescence, Vol. 12, Nos. 3/4, December 2002 (© 2002)

Probing Si and Ti Based Sol-Gel Matrices by Fluorescence Techniques

Graham Hungerford,[1,3] Mário Rui Pereira,[1] João A. Ferreira,[1] Teresa M. R. Viseu,[1] Anabela F. Coelho,[1] M. Isabel, C. Ferreira,[1] and Klaus Suhling[2]

Received May 30, 2002; revised July 31, 2002

The photophysical behavior of several probes incorporated in sol-gel–derived matrices (both monoliths and thin films) has been studied using steady-state and time-resolved fluorescence, along with fluorescence anisotropy to study the matrix structure and to elucidate probe-matrix interactions. The probes studied include laser and solvatochromic dyes along with porphyrins and phthalocyanines. It was found that spectral shifts, time-resolved decays, and quantum yields depend on the type of matrix and its preparation conditions combined with the drying time and the nature of retained solvent, which can be added to act as an anticracking agent. The differences between the results in the TiO_2 matrix, where electron transfer is most probably present, and SiO_2 are shown.

KEY WORDS: Sol-gel; fluorescence; microenvironment.

INTRODUCTION

Oxide matrices prepared by the sol-gel technique [1] have been extensively used for dye incorporation [2,3]. Low-temperature processing, good thermal inertness, increased photostability, and the possibility of controlling the porosity and pore size are clear advantages of these systems in many applications. On the other hand, because the photophysical behavior of some dyes and other organic compounds is strongly dependent on the properties of the microenvironment, absorption and fluorescence measurements can be used for the matrix characterization [4] and also to monitor the gelation and drying processes [5,6]. In particular, fluorescence anisotropy appears to be a promising tool for the study of the dynamics of nanoparticle growth [7,8], as an alternative to light scattering techniques [9].

When the oxide has semiconducting properties, as in the case of TiO_2, injection of electrons from the photoexcited species into the conduction band of the semiconductor can occur. Owing to the large surface area available for adsorption in the sol-gel nanoparticles, interesting possibilities arise for efficient photocatalytic processes [10], and applications in solar photoelectrochemical cells [11] and photodegradation of dyes [12] have been the subject of many studies. The measurement of the photophysical parameters can provide valuable insight to the elucidation of these processes.

In this paper, photophysical studies of some fluorescent molecules entrapped in both passive (silica) and active (titania) sol-gel–derived matrices obtained by alternative processing routes are reported. The probes studied include fluorescent dyes and porphyrins. In some cases additional solvents, commonly used as anticracking agents, have been added and their influence is evaluated. These studies are complemented by the measurement of the physicochemical properties of the matrices by other

[1] Departamento de Física, Universidade do Minho, 4710-057 Braga, Portugal.
[2] Department of Biological Sciences, Imperial College of Science, Technology and Medicine, London SW7 2AZ, UK.
[3] To whom correspondence should be addressed. e-mail: graham@fisica.uminho.pt

ABBREVIATIONS: DMF-*N*,*N* dimethylformamide; DMSO-dimethylsulfoxide; EG-ethylene glycol.

1053-0509/02/1200-0397/0 © 2002 Plenum Publishing Corporation

techniques, including X-ray diffraction, atomic force microscopy, and thermogravimetric analysis. This work is not intended to be a general review and refers mainly to the research performed in our group with the inclusion of some references to work carried out by other groups.

MATERIAL AND METHODS

Matrix Production

Sol-gel–derived (SGD) matrices in both thin film and monolith form were produced. Two different protocols were employed to obtain titania matrices, whilst one principal method was used to produce both forms of silica matrix. The routes used are outlined below. Overall matrices were considered ready when no further apparent changes in their size could be observed. Using the following routes, robust samples of good optical quality could be obtained. For the production of monolith samples, 10-mm pathlength plastic cuvettes were used as moulds to produce samples of approximate dimensions, 15 × 5 × 5 mm for silica and slightly smaller for titania. In the case of the thin film matrices, these were produced by dipping quartz or glass slides into the appropriate reaction mixture. All the solvents were of spectroscopic quality and all chemicals used without further purification.

Silica Matrices

These matrices were produced using the acid catalyzed hydrolysis and condensation of tetraethyl-orthosilicate (TEOS) with ethanol and water. The method used was adapted from that by Matsui and Usuki [13] and was applied with minor procedural changes to produce thin film and monolith matrix forms [14] with the inclusion of retained solvent if desired [15]. This additional solvent can at times act as a drying control chemical additive (DCCA) to reduce stresses and prevent cracking during the drying stage. The protocol is depicted in Scheme I.

Titania Matrices

In the production of titania SGD matrices two methods employing different titanium precursors were used. The first method makes use of tetraethyl-orthotitanate (TEOT) and was performed in the manner outlined in Scheme II. This route was arrived at by modifying that for the production of silica matrices. The other approach depicted in scheme III, made use of titanium (IV) isoproxide [Ti(IV)iP]; this technique is based on and adapted from methods described previously [16,17].

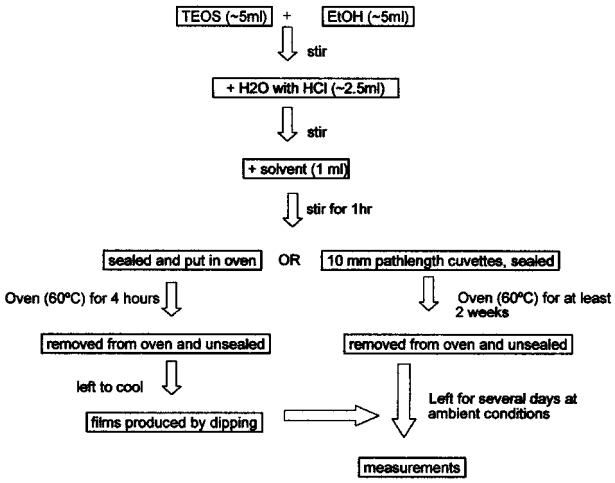

Scheme 1. Reaction route for silica thin film and monolith matrices (reaction route I).

Measurements

Characterization

The matrices were characterized using several techniques. The monolith structure was examined by X-ray diffractometry (XRD) using a Phillips PW1710 diffractrometer, with the matrices first reduced to a powder and the measurement performed in the high-angle configuration. The thermogravimetric analysis (TGA) to ascertain the presence and quantity of retained solvent was carried out using a Perkin Elmer TGA7. Analysis of the surface using atomic force microscopy (AFM) was performed in the

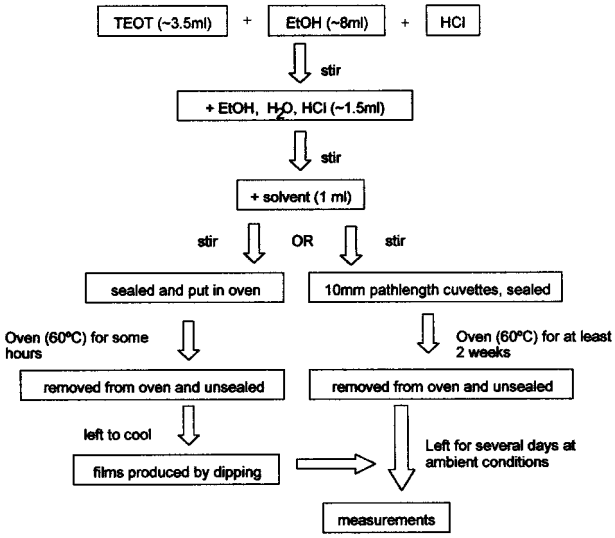

Scheme 2. Protocol for producing matrices using a TEOT precursor (reaction route II).

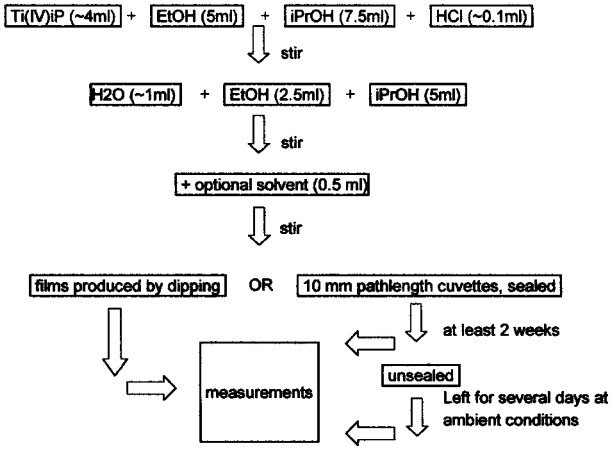

Scheme 3. Method based on Ti(IV)iP (reaction route III).

tapping mode with silicon nitrate tips using a Digital Instruments Nanoscope III.

Optical measurements

The steady-state absorption/transmittance and fluorescence emission measurements were carried out using a Shimadzu UV3101PC spectrophotometer and SPEX Fluorolog fluorimeter, respectively. Spectral analysis was done using Microcal Origin software. Time-resolved measurements were performed using the single-photon counting technique. The fluorometer excitation source was either a coaxial flashlamp operating at a repetition rate of 40 kHz or a pulsed diode controller used in conjunction with a range of LEDs (IBH NanoLED) with a repetition rate of 800 kHz. With the latter the equipment was run in reverse mode. In all cases the nominal full width at half maximum (fwhm) was about 1.5 ns. Detection was with a Hamamatsu R2949 side window photomultiplier, although for the spatial resolved measurements a 16-anode Hamamatsu H6568 photomultiplier was employed, with the output passed via a Phillips Scientific 776 amplifier and 706 discriminator to an IBH 5000MXR multiplexer-router [18,19]. The signal was acquired on an Oxford Instruments PCA3 MCA card. Instrumental profiles were measured sequentially using a scattering solution (or quartz slide) and the data analyzed using software provided by IBH Ltd. The fits were judged in terms of a χ^2 value and weighted residuals. Errors are given as three standard deviations and the preexponential components are normalized to unity. The fluorescence microscope images were produced using an image intensifier operating in the photon counting mode (Photek) in conjunction with a CCD camera (Pulnix TM-6701AN) mounted on the camera port of a transillumination microscope (Zeiss), which has been described elsewhere [20]. With this system, sub-CCD-pixel resolution can be obtained when used in conjunction with a centroiding algorithm to process the data [21,22].

MATRIX CHARACTERIZATION

Several techniques were employed to characterize the structure and morphology of SiO_2 and TiO_2 matrices, both as bulk and as film samples. X-ray diffractometry, as shown in Fig. 1 confirmed that all silica matrices are primarily amorphous. On the other hand the TiO_2 matrix (Fig. 1, diffractogram 4) clearly exhibits diffraction peaks that can be unambiguously ascribed to polycrystalline anatase. Analysis of the major peak width of graph 4 according to the method proposed by Langford [23] provided a value of 3 nm for the coherence length (characteristic length of anatase domains within the matrix) of the TiO_2. However, the presence of an additional solvent, such as, *N*, *N*-dimethylformamide (DMF), for example, appears to have a significant effect, in that it favors a less ordered structure. This shows that retained or additional solvents, added as DCCAs for example, can play an important role in determining the overall structure of the matrix, and it should be noted that it has previously been reported that the addition of DMF can enlarge the pore size [24].

Further evidence for the retention of solvents within the matrix pore structure was obtained from the near infrared (NIR) absorption spectrum, because several solvent bands can be observed. Figure 2, upper panel, shows the NIR spectrum for a silica monolith (route I) without

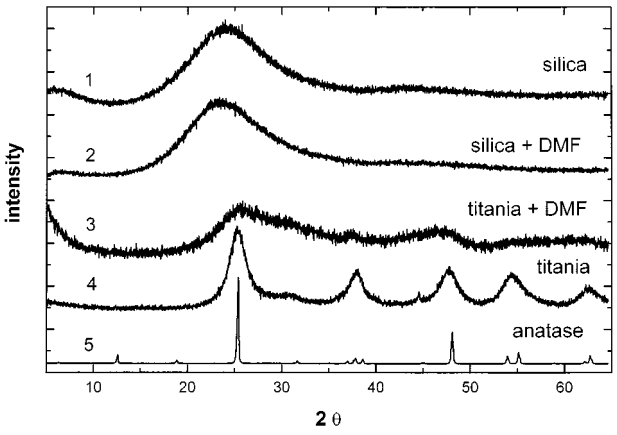

Fig. 1. X-ray diffractograms for different monolith SGD matrices, with and without DMF as an additional solvent. That for the anatase form of TiO_2 is shown for comparison. Matrices 1 and 2 were produced by reaction route I: 3 was reaction route II and 4 reaction route III.

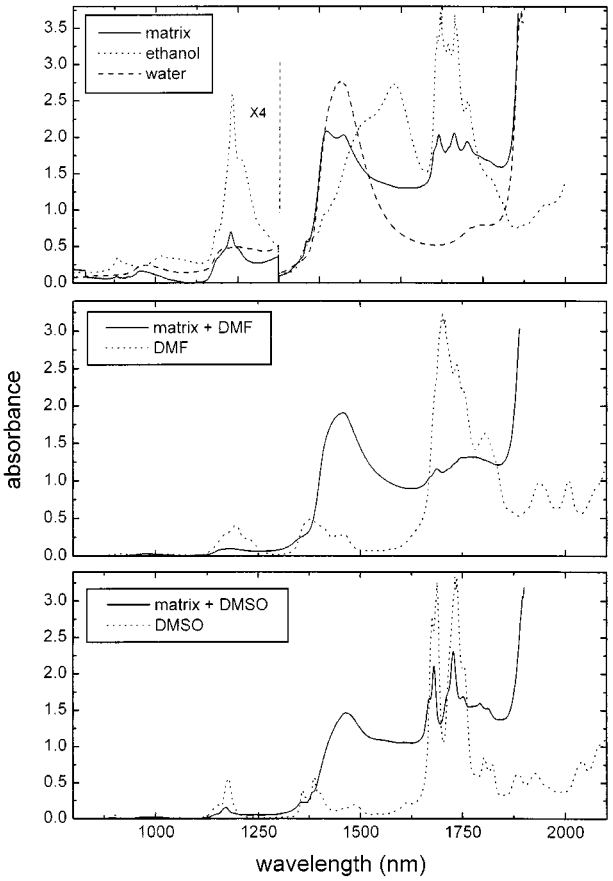

Fig. 2. NIR spectrum of a silica monolith without and with retained solvents. The spectra of selected solvents are shown for comparison.

any additional solvent. From this we can deduce the presence of some water and ethanol within the finished matrix structure. If an additional solvent is included during the manufacturing process, its presence may also be ascertained in a similar manner. The other panels in Fig. 2 demonstrate this for silica matrices with added DMF and dimethylsulfoxide (DMSO). The band structure of the solvents can be seen superimposed on that of the matrix. Evidence for the presence of solvents, even in supposedly dry matrices, was also obtained by the use of TGA, which indicated the presence of about 20% solvent by weight [14]. Repeat measurements 6 months after the initial ones showed little difference indicating that any retained solvent was confined in the matrix interior, and under these drying conditions further removal of solvent was negligible.

Complementary to determining the extent of solvent retention, it is also important to estimate the void fraction of these microheterogeneous materials. Application of an effective media theory [25], which was developed for microscopically inhomogeneous and disordered materials, to the values of the dielectric constant obtained from the transmittance spectra in the range 400–800 nm [26] (for both silica and titania, route III, monoliths) has provided data, in combination with analysis of the NIR spectrum, on the solvent and also the void fractions (in volume), as shown in Table I. According to this theory the effective dielectric constant, ε, is related to the dielectric constant of each component, ε_i, by the equation:

$$\left\langle \frac{\varepsilon_i(\omega) - \varepsilon(\omega)}{\varepsilon_i(\omega) - 2\varepsilon(\omega)} \right\rangle = 0 \qquad (1)$$

By assuming a three-component system (bulk oxide, solvent mixture, and void) the void fraction f_v could be obtained from:

$$\sum_i f_i \frac{\varepsilon_i - \varepsilon}{\varepsilon_i - 2\varepsilon} = 0 \qquad (2)$$

The data given in Table I show that, in absence of added solvents, the void fraction is greater for the titania matrices than the silica, but that the silica has a "wetter" internal environment. It is also worth noting that the void fractions of the monoliths are considerably lower than those obtained for SiO_2 thin film SGD matrices. Indeed, previous work by some of the authors has shown that up to 70% of the film could consist of void space [14], which demonstrates their porosity, a useful asset for use in sensor applications. In relation to the titania SGD films (reaction route III), these have been investigated optically [27] and their optical constants (n,k) determined from a detailed analysis of the transmittance spectrum in the range 250–2200 nm, making use of Abelès matricial method [28]. The complex refractive index (ñ) behavior was investigated via the unified treatment of Forouhi and Bloomer [29]. The calculated curve was fitted to the measured one and the best fit parameters of thickness (d), n(E), and k(E) obtained [27]. Each fit is given by the respective φ value, defined as:

$$\varphi = \left[\frac{\Sigma(T_{exp} - T_{calc})^2}{\Sigma(T_{exp})^2} \right]^{1/2} \qquad (3)$$

The measured spectrum and recovered fit parameters are

Table I. Composition of Bulk SGD Matrices Obtained from Effective Media Theory and Analysis of the NIR Spectra

Matrix	Bulk oxide (%)	Ethanol (%)	Water (%)	Void (%)
Silica	56	11	18	15
Titania	47	8	15	30

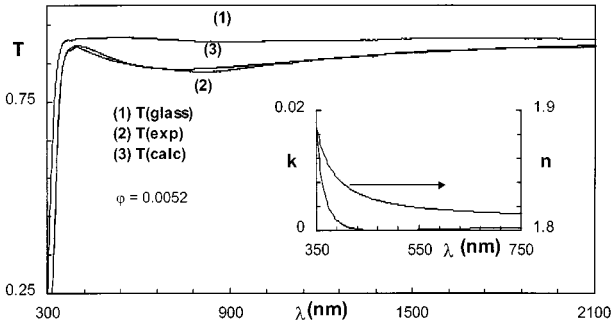

Fig. 3. Optical characterization of a titania SGD film produced by reaction route III.

shown in Fig. 3. This shows the measured transmittance of the glass substrate (1), the film on glass sample (2), and the calculated fit (3). The results obtained show the thickness to be 0.13 μm, which is *ca.* 10 times less that of the silica films where we estimate a thickness of 1.5 μm [14]: however, the void fraction (f_v) is comparable (54%). The use of Abèles treatment has also shown that the films were optically homogeneous and therefore equivalent to a single layer of a nanoporous material. This feature was further confirmed by the use of a fluorescence microscope system [20]. In fact the films produced by this technique have been found to be homogeneous, with the obvious exception of edge effects. This is demonstrated in Fig. 4a, which shows a fluorescence image of a DCM-doped SGD silica film. This method is also adept at spotting problems with the manufacturing process, as demonstrated in Fig. 4b, where sticking of the dipping device can be clearly seen by the strips in the image.

Moreover, the application of several fluorescent dyes to follow the production procedure of the films has proved useful, for example, making use of the solvatochromic probe PRODAN. In an environment of high dielectric constant (e.g. aqueous) this dye emits close to 530 nm, while in lower dielectric constant environments the emission is at a shorter wavelength (close to 410 nm). We have observed after manufacture a spectrum with a peak emission close to 510 nm and a shoulder about 430 nm. This behavior has also been described in terms of changes in the solubility of PRODAN, where upon drying there is a decrease in the monomeric form (longer wavelength emission) and the formation of aggregates [30]. In a sample measured three days after manufacture we measured the ratio of shoulder to peak as 1:4.4. However, after a period of 10 days the longer wavelength emission had decreased significantly and this ratio was roughly 1:1, demonstrating a means by which fluorescence can be used to follow the drying process.

The fluorescence anisotropy of PRODAN has previously been used to investigate the drying of thin SGD films [31] and uncovered different aspects of the process. We have also employed fluorescence anisotropy, using

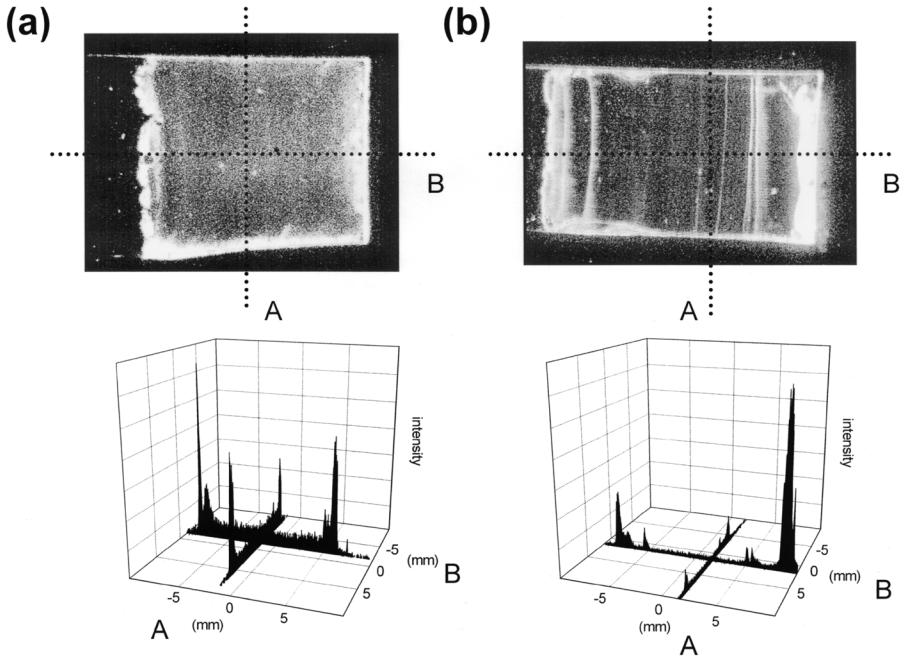

Fig. 4. Fluorescence images of silica SGD films produced by dipping (a) containing the laser dye DCM and (b) doped with R6G showing problems encountered with the dipping procedure. The plots below show the variation of intensity across the films.

in this case, Rhodamine 6G (R6G) as the fluorophore [14]. The recovered anisotropy decay and fit are shown in Fig. 5a. The results obtained gave a rotational correlation time of 2.35 ns and a high limiting anisotropy (r_∞) of 0.24. This can relate to a hindered rotation, enforced by the internal pore geometry, or even to dye adsorbed to the matrix. The fact that a rotational correlation time was obtained is indicative of the presence of some solvated dye within the matrix interior. Work by Bright and co-workers probing bulk TMOS tetramethylorthosilicate (TMOS)-derived matrices by anisotropy has revealed the presence of several environments within the matrix [5]. If we consider that the rotational correlation time just gives an indication of the viscosity of the environment, then a value of 13.2 mPas can be obtained. Thus for this type of film the dye appears to be solvated in a moderately viscous geometrically confined environment, although there is also the possibility of dye in a drier environment, adsorbed to the host.

The presence of retained solvents in the monoliths was also investigated by time-resolved spectroscopy, as shown by the analysis of time-resolved fluorescence anisotropy measurements making use of R6G [14]. This work provides evidence for the presence of retained liquid. The recovered decay is shown in Fig. 5b and on analysis required the sum of two rotational correlation times. Again assuming that these relate to two environments of differing viscosity values of 7 and 195 mPas can be recovered. These values are greater than those obtained for bulk solvent used in the manufacture and corroborate other results with similar matrices [5]. These results along with those for the composition indicate an internal matrix environment isolated from the outside.

To determine the accessibility of fluorescence probes within the finished matrix structure, we made use of the

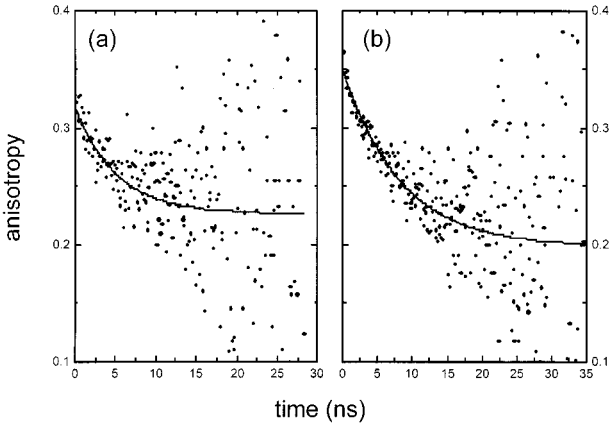

Fig. 5. Fluorescence anisotropy of rhodamine 6G in (a) a silica SGD film and (b) a silica SGD monolith.

effect of oxygen quenching of pyrene. The spectrum of this molecule incorporated into a silica matrix is shown in Fig. 6. First, from the ratio of the first and third peaks, we have an indication of the polarity of the environment [32]. The ratio obtained, 1.48, indicates a polar environment, although not as polar as that of water. In the latter a value of 1.87 has been obtained [32], whereas the value expected in a low polarity solvent, such as tetradecane, has been reported as about 0.5 [33]. The ratio we obtain is comparable to that of other work [13] using pyrene to follow the production process. Time-resolved fluorescence measurements returned decay times of 8 (0.31) and 182 ns (0.69). The bracketed numbers denote the normalized pre-exponential values. These values are similar to those obtained using pyrene derivatives in silica films, where shielding from oxygen was attributed to the presence of a layer of chemisorbed water [34]. The longer-lived, major component is indicative of an environment relatively free from the effects of oxygen quenching, though a complete absence of oxygen would probably increase this decay time further. Although a similar argument to that used in the films [34] could be applied to our monoliths, because these are less porous, so the data are indicative of pyrene more or less isolated from the external environment, with a small quantity accessible to ambient oxygen. This was further verified by monitoring the peak fluorescence emission with time when the air surrounding the sample was replaced by nitrogen. The outcome is presented in the inset in Fig. 6. This shows that the fluorescence intensity increased by close to a factor of 2 initially before settling at approximately 1.7 times the initial value. If all the pyrene was initially accessible, then this value should be several times higher, thus confirming our initial ideas that the interior of our SGD monoliths provides an apparently isolated environment in which to incorporate molecules, with poor interlinking between the external and internal pore structures.

To evaluate the matrix surface an AFM measurement was performed. A result obtained on a titania sample (made by reaction route III) is given in Fig. 7. This shows a regular surface exhibiting globular type growth forming a ramified structure, whose pores are not due to the spaces in the ramifications, but to free space resulting from the wrapping up of the nodules originated from centers of growth. These nodules have an average dimension around the 40–60 nm diameter. Analysis of the pore dimensions on the surface yield values in the order of nanometres. This contrasts with similar measurements performed by fracturing the gel, where pore diameters in the order of several tens of nanometres were obtained, hence providing further evidence for the difference between the external and internal characteristics of these matrices.

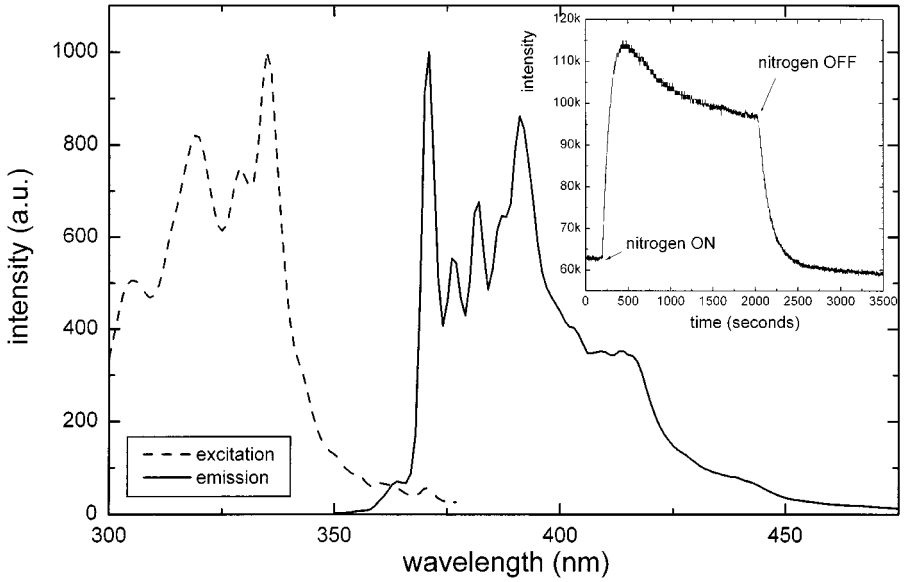

Fig. 6. Emission spectrum of pyrene incorporated in a silica SGD matrix with (inset) the effect of introducing a nitrogen environment on the peak fluorescence intensity.

PROBE AND MATRIX INTERACTIONS

In our work we have concentrated on using three main types of fluorescent molecules to incorporate within our matrix systems, namely; laser dyes, solvatochromic probes, porphyrins and phthalocyanines. The former, as well-studied highly fluorescent dyes, should demonstrate our ability to encapsulate molecules and show the suitability of the host matrix. Also we have some evidence from solution work that conditions are favorable for photoinduced electron transfer between rhodamine 6G and the titania matrix. In this case the silica matrix serves as a reference system. Solvatochromic probes such as Nile Red and PRODAN can have a dual purpose. They are ideally suited to report on the environment within the SGD matrix, and, as we have demonstrated, by changing the environment within the matrix, control can be exerted over their fluorescence [15]. Porphyrins and phthalocyanines are important models for biological systems and have potential in the field of molecular electronics. Their application, especially when combined with the electronic properties of titania, is particularly attractive because they show promise to photosensitize the host matrix. With this aim in mind we set out to produce an "active" matrix using a titanium precursor, while the silica SGD matrix was designed to act as a "passive" reference system. Thus, the study of how these molecules can be incorporated and interact with the host is of fundamental importance.

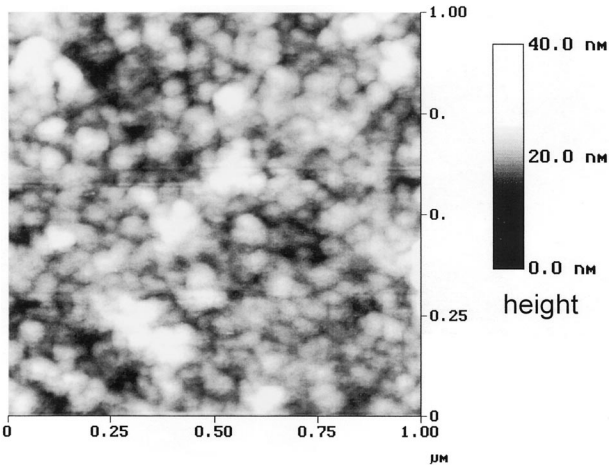

Fig. 7. AFM image of the surface of a titania SGD monolith (made via route III).

Rhodamine 6G

This well-known laser dye proved an attractive initial choice because of its stability, high quantum yield in silica SGD matrices [2], the fact that compartmentalization in these matrices favors the monomeric form (diminishes aggregation) [35], and solution studies indicate that suitable conditions exist for electron transfer between the dye and the titania host. Previous work has made use of this dye to study TMOS-derived thin film [36] and bulk [5] matrices. An initial study involved checking the effect of different concentrations of dye loaded into both thin film and monolith types of silica matrix and both the

steady state and time-resolved behavior monitored [14]. A summary of the fluorescence data is given in Table II. This shows that overall there is an increase in emission wavelength with increasing dye concentration. The time-resolved data from the films can relate to the presence of a limited number of solvated sites (giving rise to the 4.3-ns component), which become filled, forcing the dye into less preferred regions (shorter component). On increasing concentration the proportion of the shorter-lived fluorescence therefore increases.

The effect of concentration is also pronounced in the monolith matrices, where the existence of rise-times (negative pre-exponential components) can be seen. This behavior is highly indicative of the self-absorption and re-emission of light, which can occur if there is an overlap between the absorption and emission spectra and a reasonable dye concentration [37]. The fact that the dye can be compartmentalized (thus restricting collisional de-excitation and bimolecular interactions) and the observation of some self-absorbed and re-emitted light indicates that the SGD matrices can provide model systems that can prove useful in the study of this phenomenon. We have performed some initial studies (both steady state and time-resolved), which we hope to explore further in the future. Figure 8a shows our preliminary steady-state measurement using a fluorescence microscope [20] to compare a dilute ($\sim 10^{-6}$ M) and concentrated ($\sim 10^{-3}$ M) R6G-doped SGD monoliths. For the lower-concentration sample the intensity behavior is quite uniform, but for the higher-concentration sample there is a sharp decrease, which relates to a large light absorption coefficient. This trend has also been observed for inner filter effects in a fiberoptic fluorimeter [38]. Figure 8b depicts the outcome of a multiplexed time-resolved measurement performed via an array of 16 optical fibers to produce a spatially resolved fluorescence lifetime map, in a manner similar to that described by Birch and co-workers [18], using a concentrated sample. The data have been treated to produce a contour map from the average decay times, obtained from a biexponential fit to each of the 16 decays. The times recovered are far in excess of that for the sample in the absence of the self-absorption and re-emission phenomenon ($\sim$4.3 ns) and hence demonstrate the suitability of these systems to study this effect.

R6G was also used (as a donor) in conjunction with two other molecules to study dipole–dipole energy transfer in order to investigate confinement effects within silica matrices, with and without retained solvent (in this case DMF). In the former the acceptor was malachite green (MG), and in the latter, zinc meso-tetra (4-sulfonatophenyl) porphyrin dihydrochloride (ZnTSPP) was used. In both systems there was a good overlap between the R6G emission and the absorption of the acceptor, thus energy transfer via the Förster mechanism is favorable. From the overlap between the R6G emission and acceptor absorption spectrum in SGD matrices R_o values (distance for 50% efficiency of energy transfer) of 43 Å and 49 Å were obtained for R6G-MG and R6G-ZnTSPP, respectively. Time-resolved fluorescence was used to monitor the R6G fluorescence for different samples containing a fixed concentration of R6G (donor) and increasing concentrations of acceptor (MG or ZnTSPP) and the resultant decays modeled using a Förster function for a three-dimensional random distribution of acceptors, given below.

$$I(t) = I_o exp[-t/\tau_o - 2\gamma(t/\tau_o)^{1/2}] \quad (4)$$

Where

$$\gamma = [A]\ (2\pi^{3/2}\ N\ R_o^3)/3000 \quad (5)$$

From these data (in all cases, acceptable fits, in terms of χ^2 value, were obtained) plots of γ against acceptor concentration, [A], were made, and the outcome is shown in Fig. 9. In the case of the system R6G-MG for SGD

Table II. Peak Fluorescence Wavelength and Decay Times from R6G–Doped Thin Film and Monolith Silica Matrices. For Errors and Explanation of Analysis see ref. [14]. Decay Times Are in ns and Emission in nm. Preexponentials (α) are Normalized and the χ^2 Value for Goodness of Fit Acceptable in All Cases

Conc (mM)	λ_{em}	τ_1	α_1	τ_2	α_2	λ_{em}	τ_1	α_1	τ_2	α_2
0.004						546	4.34	1		
0.021						556	5.56	1		
0.06	542	2.08	0.44	4.30	0.56					
0.21						570	2.95	−0.13	6.18	0.87
0.24	545	310	0.47	4.30	0.53					
1.2						594	6.21	1		
1.6	548	3.13	0.68	4.30	0.32					
2.0						607	0.33	−0.33	6.37	0.67
4.9	550	2.20	0.95	4.30	0.05					

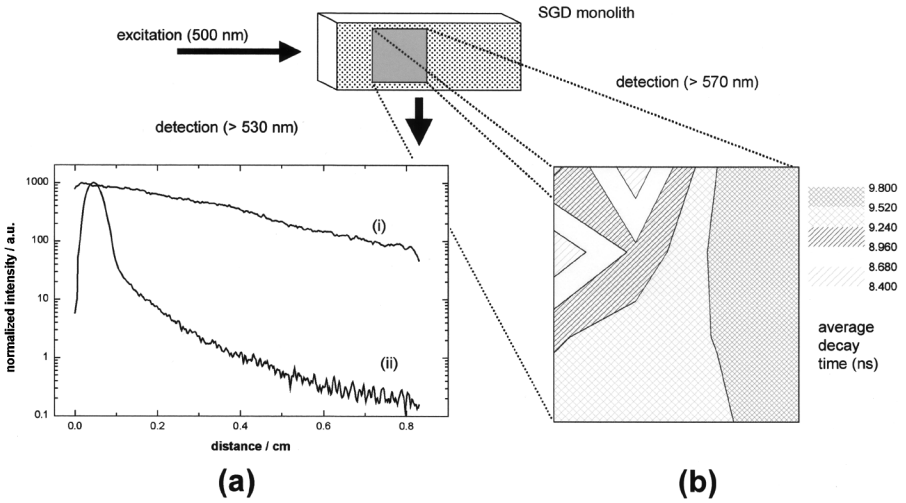

Fig. 8. Silica SGD monoliths doped with rhodamine 6G (a) steady-state intensity data for (i) a dilute amount of dye, (ii) a concentrated quantity, and (b) contour map generated from a time-resolved study.

matrices without DMF the plot does not fit to a single straight line, but requires two [14]. The gradients produce R_o values of 104 Å and 67 Å, both of which are greater than that obtained from the overlap integral (43 Å). However, the smaller value is close to that obtained experimentally with this dye combination adsorbed to a vesicle surface [39]. The larger value indicates that the energy transfer process is more efficient (*ca.* 200 times considering the value of 104 Å and 14 times for the value of 67 Å) than expected. This can relate to geometrical confinement within the matrix producing a higher local acceptor concentration, coupled with a pore size distribution. However some caution should be exercized in interpretation, because it is quite likely that there is a non-uniform acceptor distribution. For the system with retained DMF, the measured R_o value (71 Å) is also larger than that calculated from the spectral overlap (about nine times more efficient). Confinement by the matrix is the most likely explanation, and although these are preliminary results using the R6G-ZnTSPP system, it is also tempting

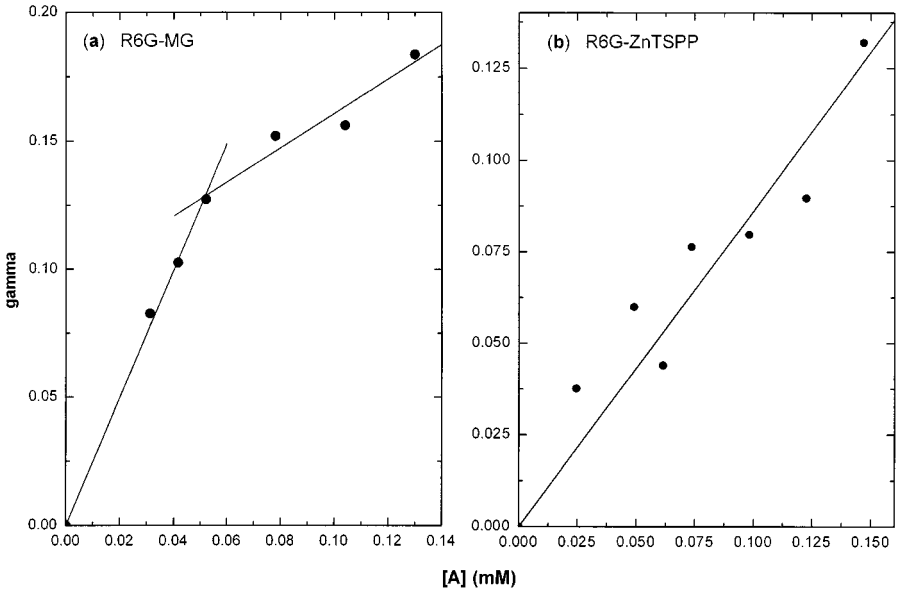

Fig. 9. Plots of gamma vs. acceptor concentration for (a) silica monoliths using R6G and malachite green and (b) silica monoliths with retained DMF using R6G and ZnTSPP.

to attribute a smaller pore size distribution to this matrix form, along with an overall larger pore diameter in relation to the matrices without retained solvent. This is expected because there is no clear-cut case for using two gradients in the R6G-ZnTSPP system, along with reduced increase in efficiency for the energy transfer process. This is not too surprising because there is a report of using DMF as a DCCA, in which a larger, more uniform pore structure was produced [24]; however, this is an area that we wish to investigate further, and treatment of the results using other models, a stretched exponential function [40,41] for example, may prove helpful in the analysis of these data.

Finally, in relation to this laser dye, we have obtained evidence in solution that conditions are favorable for photoinduced electron transfer between R6G and TiO_2 [42]. The redox potentials of R6G were determined by cyclic voltametry using a scan rate of 100 mVs^{-1}, with the dye in aqueous solution with a large excess of KCl. In relation to an SCE, an oxidation potential of +1.10 V and a reduction potential −0.81 V were obtained [42]. To see if this solution study translates to our matrix systems and to obtain a rate, a time-resolved fluorescence study was undertaken using either the silica (reaction route I, with and without DMF) or solution measurements as the reference value compared to the decay times obtained from R6G in titania matrices, made using routes II and III. Assuming that any quenching occurred via electron transfer from the R6G to the titania matrix the rate (k_{et}) was calculated using Eq. 6.

$$k_{et} = 1/\tau - 1/\tau_{ref} \quad (6)$$

The results obtained are given in Table III and show that a significant decrease in decay time is observed in the titania samples. Unsurprisingly a greater decrease observed in the sample without retained solvent as the presence of DMF is expected to diminish dye-matrix interactions. Further studies are required to fully verify these data.

DCM and 4-Di-1-ASP

The laser dye DCM is well studied [43,44] and is noted because it exhibits a large Stokes' shift and has a good photostability [45]. Thus this dye appears a good choice for incorporation into SGD matrices, and there are reports in modified sol-gel systems [46,47]. However, we have found that on incorporation into matrices using reaction route I this dye becomes protonated by the acid catalyst [48]. A similar fate occurred when incorporating the dimethylamino-stibazolium dye 4-Di-1-ASP (pyridinium, 4-(2-(dimethylamino)phenyl)-1-methyl, iodide) into our silica matrices. This is also a dye that has been reported as having solvent-dependent behavior [49] and could be used with microheterogeneous systems [50]. Figure 10 demonstrates the effect of an acid on the spectra of 4-Di-1-ASP. In the case of DCM a similar behavior is observed, which relates to protonation of the dye [48], with both a dramatic decrease in the main longer wavelength absorption and an increase in shorter-wavelength bands. The peak emission, although situated about the same peak wavelength is considerably reduced in intensity.

Having shown that it is possible to incorporate solvents within the monoliths internal pore structure, we decided to make use of this fact and to add aprotic solvents, which should help to alleviate the effects of the acid catalyst, to our reaction mixture (route I). In this case DMF and DMSO were chosen. Figure 11 shows the fluorescence spectrum of DCM in both solvent and SGD matrices (both with and without retained solvent). The spectrum obtained without retained solvent is blue shifted in relation to those in the other matrices or in pure solvent. It is also at shorter wavelengths than that observed in ethanol [51], to which the interior of TEOS-derived matrices have been likened [3]. Also the intensity of the emission is very much reduced in relation to the others (spectra shown relative for ease of comparison). We have also noticed this type of behavior for concentrated DCM in

Table III. Fluorescence Decay Data for R6G Incorporated in Silica and Titania SGD Matrices and Calculated Rate for Electron Transfer. Decay Times are Given in ns

Matrix	DCCA	Route	τ_1 (ns)	α_1	τ_2 (ns)	α_2	χ^2	k_{et} ($\times 10^8$ s^{-1})[b]
DMF[a]			3.82 ± 0.02	1			1.10	
Silica		I	4.34 ± 0.02	1			1.09	
Silica	DMF	I	4.26 ± 0.02	1			1.19	
Titania		III	0.98 ± 0.07	0.62	2.77 ± 0.03	0.38	1.14	3.72
Titania	DMF	II	0.70 ± 0.42	0.18	3.03 ± 0.03	0.82	1.05	1.48

[a]Solution study.
[b]Obtained from average decay time and Eq. 6 with corresponding silica reference.

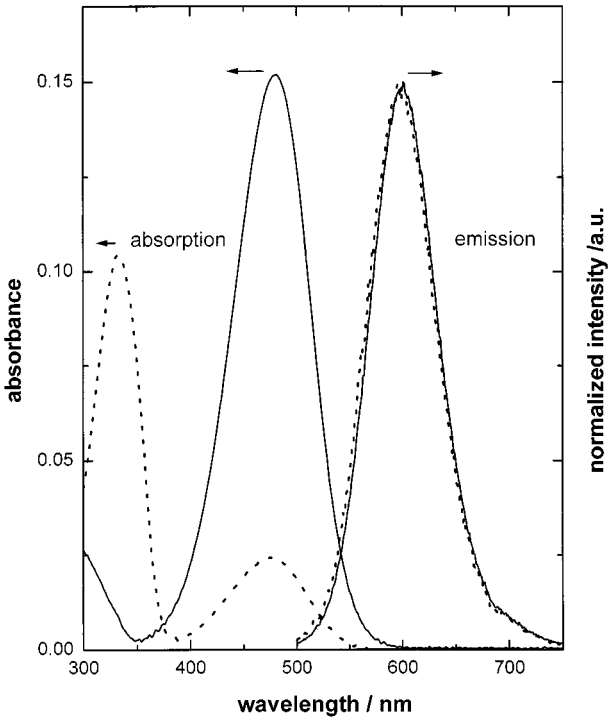

Fig. 10. Effect of concentrated HCl on the absorption and fluorescence spectra of 4-Di-1-ASP. (——) in ethanol (- - -) in ethanol + HCl.

silica SGD thin films, and thus another possibility is that the emission originates from DCM adsorbed on the bulk oxide or in an aggregated form. In the matrices with retained solvent the emission is closer to that observed in pure solvent. Only a small reduction in yield and a slight blue shift in the peak emission are seen relative to the pure solvent, and from this we deduce that the DCM is in fact solvated in the retained solvent, within the monoliths internal pore structure. Time-resolved measurements (Table IV) [48] seem also to indicate that this is a realistic hypothesis because the values are similar to those in solution.

Table IV. Recovered Decay Parameters for *ca.* 5×10^{-5} M DCM in the Different Systems Analyzed as a Sum of Exponentials. The Excitation Wavelength, was 490 nm and the Emission was Selected Using a 570-nm Cut-off Filter

Retained Solvent	τ_1 (ns)	α_1	τ_2 (ns)	α_2	χ^2
DMF	1.01 ± 0.05	0.79	2.31 ± 0.05	0.21	1.16
DMSO	1.15 ± 0.09	0.67	2.29 ± 0.04	0.33	1.14

Considering 4-Di-1-ASP, this (qualitatively) appears to survive incorporation into silica SGD matrices better than the DCM. This could be a consequence of the DCM being hydrophobic, while the 4-Di-1-ASP is soluble in water. The fluorescence data are given in Figure 12. The steady-state spectra exhibit a slight red shift in the matrices with DMF, indicative of an environment with a higher dielectric constant, as expected [15]. A difference is also observed in the excitation spectrum, which requires further investigation to elucidate the role of interaction with the host material. In ethanol this dye is reported to have a lifetime of ~50ps [49], but this appears to increase on

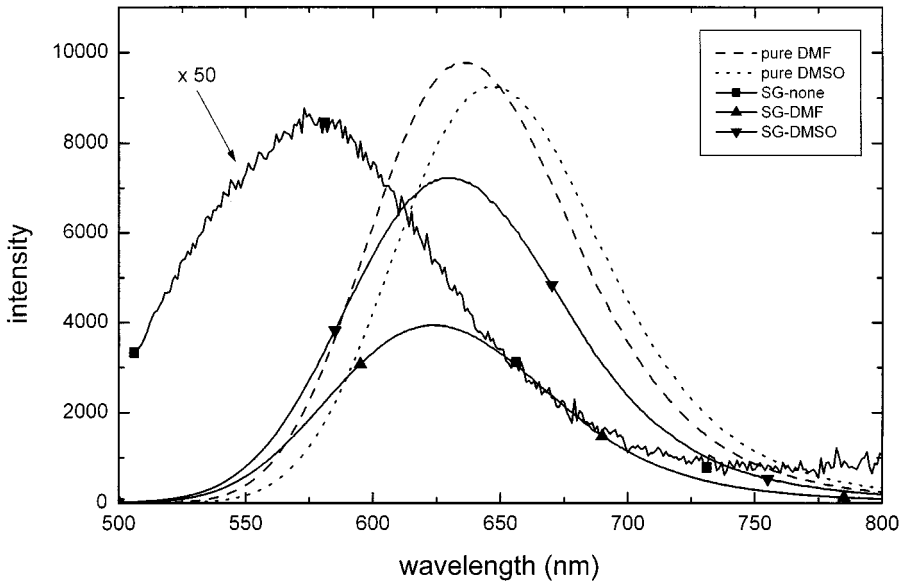

Fig. 11. DCM emission in both pure solvent and SGD matrices without retained solvent (none) and with DMF or DMSO. The intensities are relative.

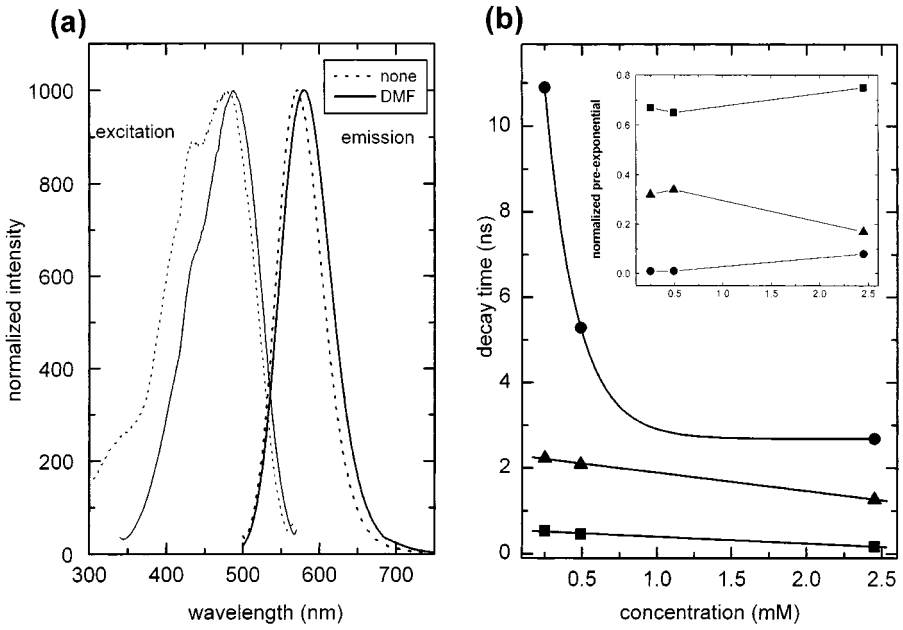

Fig. 12. 4-Di-1-ASP incorporated in silica SGD matrices (a) steady-state and (b) decay time data in a matrix without additional solvent.

incorporation into the SGD matrices. We required a sum of three exponentials to fit the data for each of the three concentrations studied (Fig. 12b). In each case the dominant component is a short-lived decay, but a significant amount of a lifetime of about 2 ns is also observed. A small (possibly negligible at low concentrations) quantity of a longer-lived decay is also present, and further work is required to assign these decay times.

Nile Red and PRODAN

The hydrophobic solvatochromic dye Nile Red has been investigated in polymer [52], protein [53], and surfactant systems [50], as well as in our silica (route I) monolith systems with retained solvent [15]. PRODAN is a solvatochromic probe with a large wavelength range for the peak emission (over 100 nm between environments of low and high dielectric constant) [50]. It has been employed as an anisotropy probe to monitor the drying of SGD thin films [31] and also to report on the internal environment within bulk TEOS-derived glasses with aging, where both polarity and viscosity data were obtained [30]. We have made use of both of these dyes to monitor the internal environment of our monolith SGD matrices obtained via each of the reaction routes. We have also endeavored to take advantage of the solvatochromic properties of these probes by altering the internal microenvironment of our matrices to tune the fluorescence of these molecules.

Nile Red and PRODAN have both been used in our titania (reaction route III) matrices to monitor the manufacturing process. Figure 13 shows in the case of the Nile Red–containing matrix, that in the "wet," or newly made, SGD matrix it exhibits a peak emission that is dependent on the excitation wavelength, indicating the probe encounters spread of microenvironments (in terms of dielectric constant). In the finished matrix this dependency is negligible, indicating a more uniform environment with a lower dielectric constant. The PRODAN data also shows a variation with time after preparation. However, in this case the results report an increase in the dielectric constant of the host medium. The difference between these two probes may be explained by the hydrophobic nature of Nile Red, while PRODAN is soluble in a wide range of solvents. Thus a combination of both studies is useful to provide the complete characterization of this system.

We have made use of retained solvents for a dual purpose, to perform as DCCAs and to modify probe–matrix interactions and hence influence the probe fluorescence. This is exemplified by the use of Nile Red in the silica matrices [15]. In this case the retained solvents were shown to be able to tune the emission of the dye within the matrix, as given in Fig. 14. When using DMF and DMSO the dye–matrix interactions were minimized and the Nile Red appeared solvated in the retained solvent within the internal pore structure of the matrix. Similar results are obtained using PRODAN (Fig. 15).

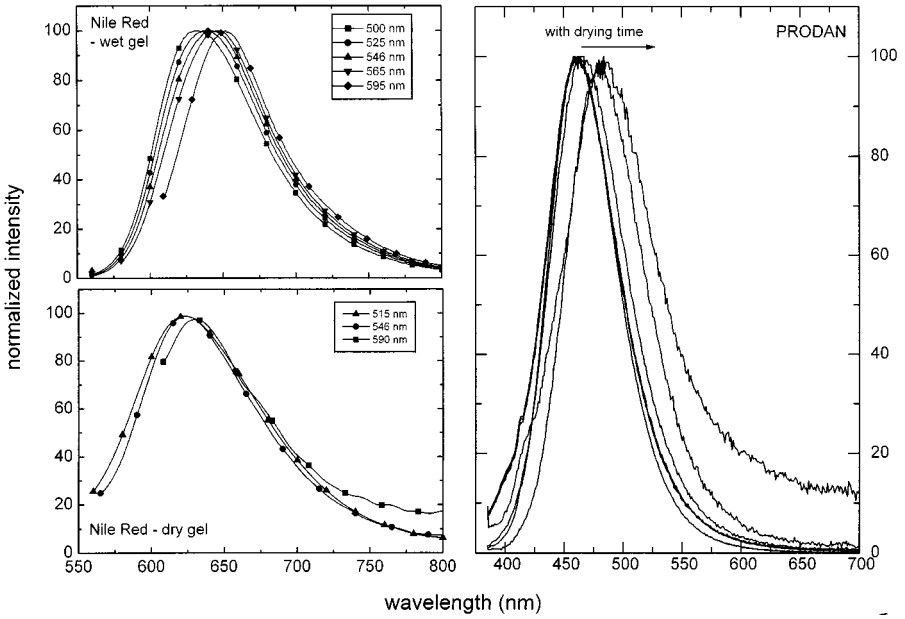

Fig. 13. Fluorescence emission of Nile Red and PRODAN in titania (route III with DMF) monoliths with time. Wet gel refers to freshly made sample, and dry gel refers to the finished matrix.

The use of DMF provides a more uniform environment for the probe, which is evident from the fact that the peak emission is approximately the same. Without retained solvent this varies over a range of nearly 20 nm, indicating a range of microenvironments. Also shown is the use of a high probe concentration, employed to attempt to access a complete range of sites within the matrix (it is likely that only the more favorable sites are populated at low concentrations). The resultant spectrum consists of two main emissions, one close to 435 nm and the

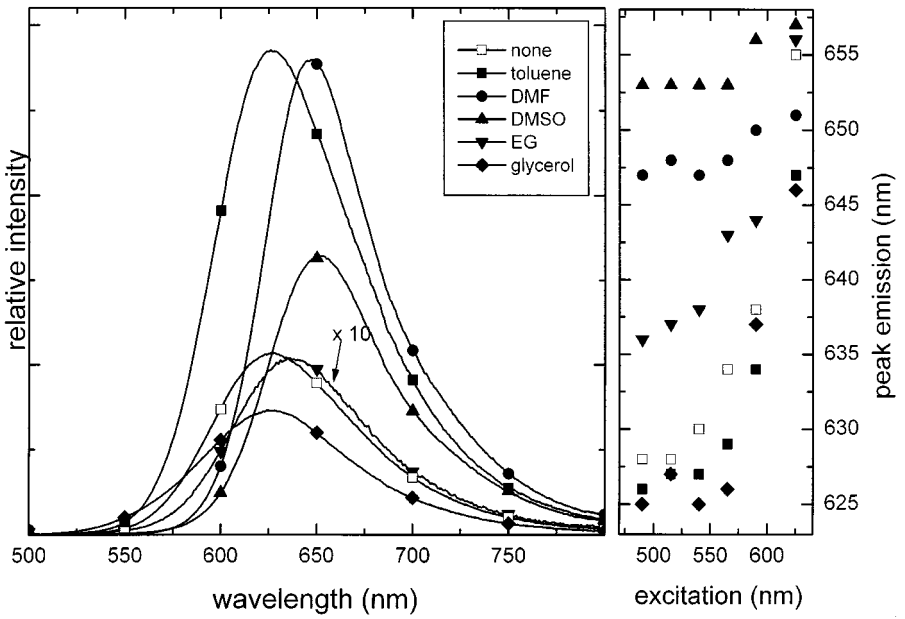

Fig. 14. Fluorescence of Nile Red in silica SGD matrices with retained solvents. The intensities of the spectra are relative, and the panel on the right-side shows the change in peak fluorescence with excitation wavelength.

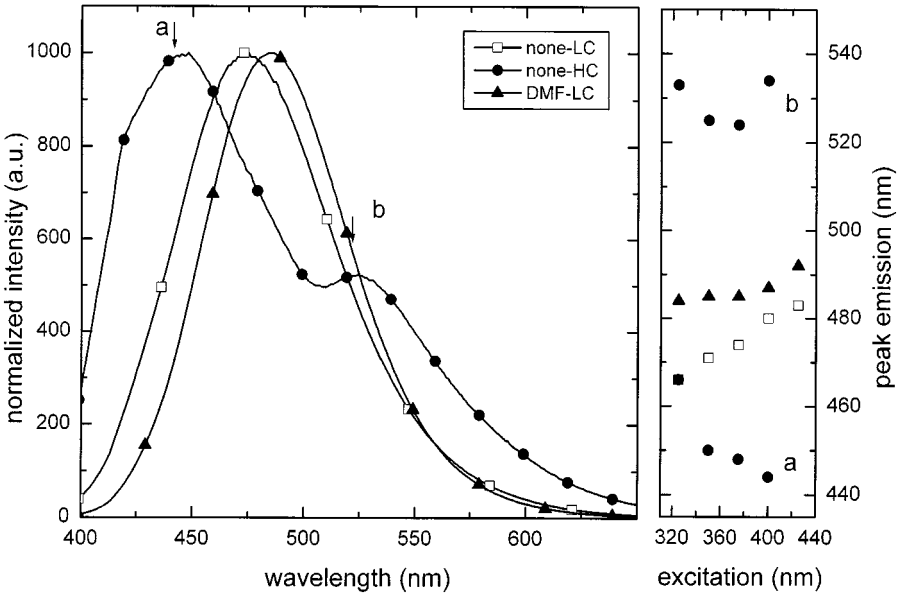

Fig. 15. PRODAN emission from matrices both without and with retained DMF. In the former a low concentration (LC $\sim 10^{-5}$ M) and a high concentration (HC $\sim 10^{-3}$ M) were used. The side panel shows the effect of excitation wavelength on the peak emission.

other near 530 nm. This is similar to that previously reported for this probe and a TEOS derived matrix, albeit produced by a different route [30]. In that work the emissions were attributed to both monomer (longer wavelength) and aggregate (shorter wavelength). Our spectrum also exhibits some shoulders, so to obtain further information it was fitted to the sum of several Gaussian spectra (five were required to produce an acceptable fit) in a manner previously employed with microemulsions containing PRODAN [33]. The outcome is given in Fig. 16, and the component spectra can relate to PRODAN occupying a range of microenvironments; from the low dielectric constant of the bulk oxide material to an aqueous-like one (PRODAN in water emits about 520 nm) of solvent remaining within the finished matrix structure. The peak emission of the lower-wavelength component spectrum (418 nm) is, in fact, close to that obtained for the TEOS precursor (417 nm), and the peak emission of another component is just slightly lower than that of the probe in ethanol (486 nm). These dyes have also been employed with titania monoliths produced via route II, and again the results (Fig. 17) demonstrate a narrow range of peak emission wavelengths, which indicates a fairly homogeneous probe environment.

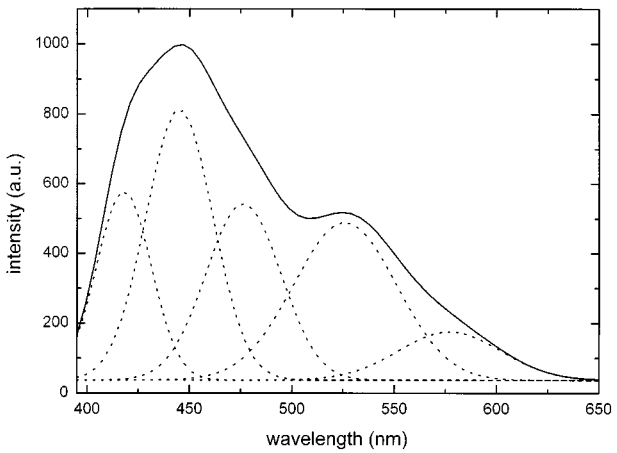

Fig. 16. Fitted spectrum and component Gaussian spectra for $\sim 10^{-3}$ M PRODAN in a silica SGD matrix.

To complement the steady-state work, time-resolved measurements were performed and the outcome using Nile Red is presented in Table V, which shows that in all cases the decays are non-exponential, contrary to that found for Nile Red in non-viscous solution [15]. For viscous solutions (ethylene glycol [EG] included), a sum of two exponentials was required and the presence of a solvent relaxed state reported [54]. Overall the data from Nile Red appear to report a raised solvent viscosity associated with the small pore diameter. The unsurprising exceptions are the data for the titania (route III) matrices, which were measured close to the beginning of the manufacturing process. This was done because the fluorescence yield of the Nile Red in the finished

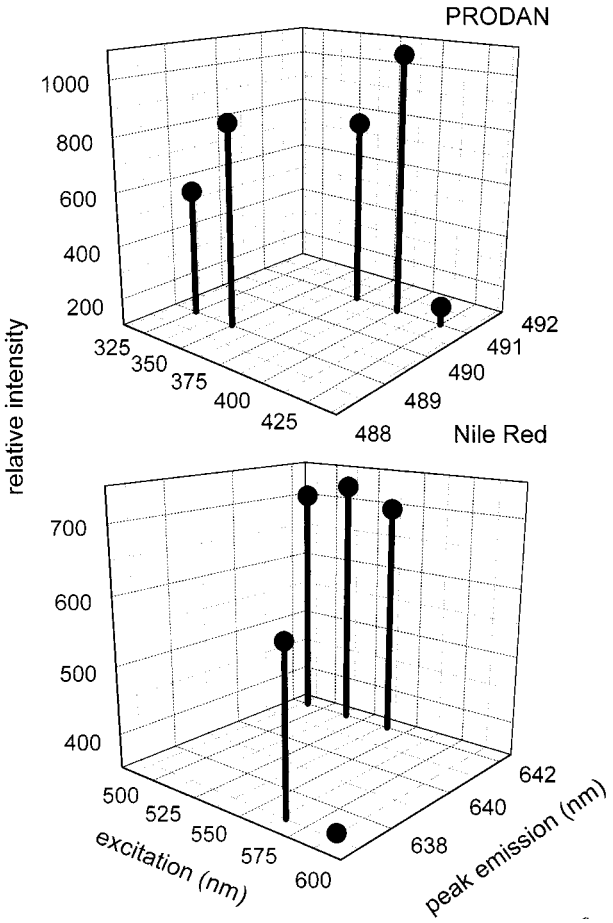

Fig. 17. Steady state fluorescence data from PRODAN and Nile Red in titania monoliths (route II) with retained DMF.

matrices precluded time-resolved measurements. This could be put down to degradation of the probe during the manufacturing process, thus the lifetime values presented relate to a relatively (in comparison to the finished matrix) low viscosity environment, similar to bulk solvent.

Porphyrins and Phthalocyanines

Both porphyrins and phthalocyanines have found application in photodynamic therapy [55] and are attractive choices for use as models for biological studies and molecular electronics. Because of this we chose to study their incorporation into SGD matrices, with possible sensitisation of the titania matrices borne in mind. To this end both the sulfonated porphyrins meso-tetra (4-sulfonatophenyl) porphine dihydrochloride (H_2TSPP) and ZnTSPP, along with several non-sulfonated (meso tetra phenyl) metal porphyrins, including GeMeOHTPP, Co(II)TPP, Fe(III)TPP, MgTPP, and AlOHTPP, were incorporated into SGD host matrices. Some of the samples were prepared with DMF as a DCCA and others prepared without any extra solvent. Using our reaction protocols the main problem on incorporation in sol-gel matrices relates to the reaction conditions (e.g., pH) required for the reaction to take place. The need for acidic catalysis forces us to drop the pH to levels that resulted, both in protonation of the H_2TSPP and in some demetallation of the other porphyrins. The former was observed by a change in the emission spectrum and a decrease in the decay time (from ~10 ns to ~5 ns) [26]. This was further verified by exposing a monolith containing H_2TSPP to ammonia gas, which should have the effect of neutralizing the acid form and reverting the porphyrin back to the unprotonated form. This was in fact what we observed using time-resolved spectroscopy and is demonstrated pictorially in Fig. 18. In the same study using both silica and titania (route III) monoliths demetallation of ZnTSPP was observed, along with evidence of protonation. On exposure to ammonia the resultant fluorescence spectrum resembled that of a metal free porphyrin, a process also mirrored in the time-resolved data [26]. The fact that the porphyrins show such behavior in these matrices in the presence of different pH conditions can prove useful for sensor applications [56].

Table V. Decay Times for Nile Red Incorporated in the Different Final SGD Monoliths. The Exception Is for the Titania Route III Values, Which Were Obtained Close to the Start of the Manufacturing Process

Matrix (route)	Retained solvent	τ_1 (ns)	α_1	τ_2 (ns)	α_2	τ_3 (ns)	α_3	χ^2
Silica (I)	None	3.65 ± 0.27	0.12	2.75 ± 0.35	0.49	0.29 ± 0.12	0.39	1.12
	Toluence	3.46 ± 0.02	0.78	0.48 ± 0.24	0.22			1.19
	DMF	3.13 ± 0.02	0.64	0.19 ± 0.12	0.36			1.12
	DMSO	3.41 ± 0.02	0.52	2.20 ± 0.32	0.48			1.19
Titania (II)	DMF	2.66 ± 0.03	0.76	1.39 ± 0.30	0.24			1.14
	EG	2.87 ± 0.09	0.04	1.03 ± 0.15	0.26	0.18 ± 0.11	0.70	1.14
Titania (III)	None	3.75 ± 0.01	1					1.14
	DMF	3.72 ± 0.01	1					1.14

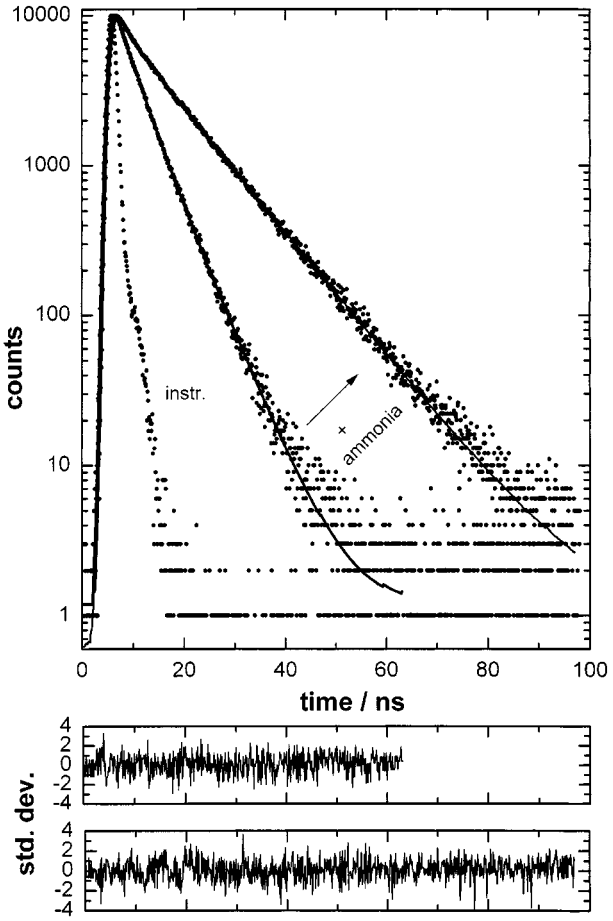

Fig. 18. The effect of ammonia gas on the time-resolved decay of H_2TSPP in a silica monolith.

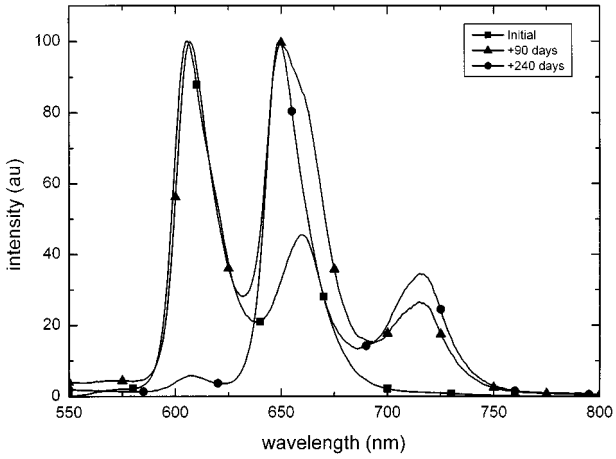

Fig. 19. Demetallation of MgTPP during the manufacture of a titania SGD matrix (route III), as seen via the emission spectrum.

In the case of the non-sulfonated metal porphyrins some demetallation was also observed. An example of this occuring with time is given in Fig. 19 for MgTPP, where with time, the emission bands progressively shift to longer wavelength to give a spectrum similar to that of a metal free porphyrin. The demetallation process can be observed by the changes in the Soret band position, as well as in the Q band region, where an increase in the number of bands is seen [57]. The emission spectra exhibit changes as well, with an increase in the Stokes' shift observed and differences in band positions. Also fluorescence lifetime measurements can be employed to follow and quantify the demetallation process. The metal species normally exhibit lifetimes that range from 1 to 8 ns for the monomeric form, while that for a hydrogen porphyrin is in the order of 10 ns, which results from the lower nitrogen coordination in the porphyrin inner core.

Table VI presents time-resolved data obtained for these porphyrins when incorporated in titania sol-gel matrices and shows that the decay kinetics are dominated by either a demetallated (longer-lived component) or a shorter-lived subnanosecond component. In the case of MgTPP (in ethanol we have measured a lifetime of 6.8 ns), the presence of DMF does indeed play an important role in diminishing demetallation, although this could be at the expense of aggregate formation, which could be manifest by the presence of a subnanosecond decay component. Further work is in progress to ascribe the origin of these decay components and porphyrin-matrix interactions have also to be considered. As we have previously shown, DMF also reduces interaction with the matrix, which is not necessarily desirable in this case and the extent of this reduction in the case of porphyrins still needs to be determined. Relating to the other metal porphyrins, both the Co(II)TPP and the Fe(III)TPP doped SGD monoliths exhibited a very low level of fluorescence (probably because of the heavy central metal atom), which precluded lifetime measurements. The aluminium porphyrin AlOHTPP, on the other hand, was found to be very stable in the acidic conditions required for our sol-gel process and showed no signs of demetallation during the incorporation procedure. In the final dry matrix the fluorescence kinetics of AlOHTPP show a clear biexponential decay, with a shorter lifetime of about 4 ns and a longer lifetime of 6.7 ns. These are similar to those of the porphyrin in DMF (Table VII) and as ascertained previously, show that the porphyrin is predominantly solvated in DMF, which is retained within the internal pore structure. We also evaluated several phthalcyanines and ClAlPc, which has a high solubility in both alcohol and DMF, plus a good quantum yield, 0.68 [58]. This was found to be stable in the matrix forming reaction conditions and displayed no signs of aggregation, even at relatively high concentrations. Previous doping of SGD

Table VI. Time-Resolved Fluorescence Data for Various Porphyrins Incorporated into Titania (Route III) Monoliths

Porphyrin	DMF	τ_1 (ns)	α_1	τ_2 (ns)	α_2	τ_3 (ns)	α_3	χ^2
MgTPP	√	0.58 ± 0.02	0.71	3.17 ± 0.14	0.20	10.14 ± 0.07	0.09	1.09
MgTPP	x	0.73 ± 0.09	0.26	6.40 ± 0.44	0.32	11.25 ± 0.07	0.42	1.11
GeMeOHTPP	x	1.26 ± 0.31	0.12	7.56 ± 0.18	0.36	11.55 ± 0.34	0.52	1.14
AlOHTPP	√	3.52 ± 0.88	0.22	6.78 ± 0.07	0.78			1.09

matrices using copper phthalocyanine have reported dimerisation relating to the synthesis conditions [59].

It should be noted that demetallation can also be avoided by incorporation of the porphyrin after the manufacture of the host. We have incorporated (using route III thin films) a metal porphyrin into a finished matrix and have observed anchoring of both monomeric and aggregated forms of the porphyrin to the titania host with no discernable demetallation [27]. The method employed, although possible for films, had the drawback that it was not readily applicable to monolith matrices.

As both the aluminium containing porphyrin and phthalocyanine appeared to exhibit the required stability, we decided to investigate these further, especially as the porphyrin emission has a reasonable overlap with the phthalocyanine absorption (Fig. 20), thus making them a potential system in which to study energy transfer via the Förster mechanism. The overlap integral (calculated from these spectra) returned a value of 30 Å for R_o. A preliminary study was made incorporating the porphyrin (donor) and phthalocyanine (acceptor) into titania (route III) monoliths, with DMF as the additional solvent. These systems have the potential for monitoring the drying process and the possibility of sensitizing the titania host. Here we will highlight a few results with the emphasis on the titania matrix.

The porphyrin absorption spectra (Fig. 21a) in the titania monolith exhibit a red shift in the Soret band, with

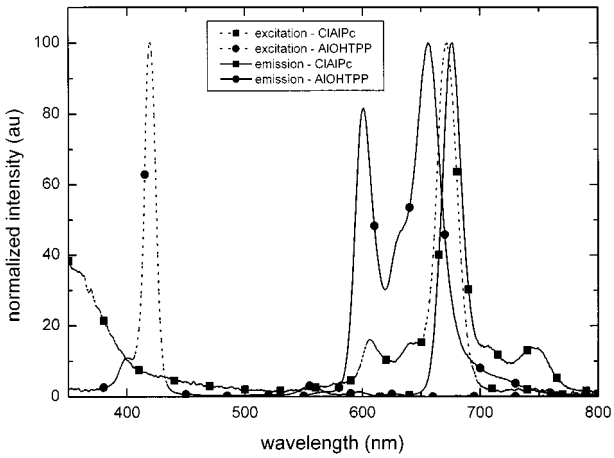

Fig. 20. Steady-state excitation and emission spectra of AlOHTPP and ClAlPc in ethanol.

drying accompanied by a broadening. Also at the final drying stage a band at 409 nm, which is only present in the sample with the porphyrin by itself, is observed. A solution study (in ethanol) showed this band to be present at high concentrations. Thus it appears that the shrinkage of the matrix during the drying stage is leading to increased AlOHTPP concentrations and the formation of aggregates. However it is interesting to note that the presence of phthalocyanine disrupts the formation of this type of aggregate. Turning our attention to the longer-

Table VII. Time-Resolved Data for the Aluminium Porphyrin and Phthalocyanine in Titania Matrices (with DMF) and in Solution

System	λ_{exc}	τ_1 (ns)	τ_2 (ns)	α_1	α_2	χ^2
Titania (route III)						
AlOTPP	586	3.52 ± 0.88	6.78 ± 0.07	0.22	0.78	1.09
ClAlPc	610	6.36 ± 0.03		1		1.12
AlOHTPP/ClAlPc	586	3.34 ± 0.88	5.98 ± 0.07	0.23	0.77	0.97
Ethanol						
AlOHTPP	586	3.77 ± 1.04	7.40 ± 0.08	0.23	0.77	1.05
ClAlPc	610	6.71 ± 0.03		1		1.19
DMF						
AlOHTPP	586	3.47 ± 0.29	6.90 ± 0.06	0.11	0.89	1.07
ClAlPc[(a)]		9.7		1		

[(a)]Reference [58].

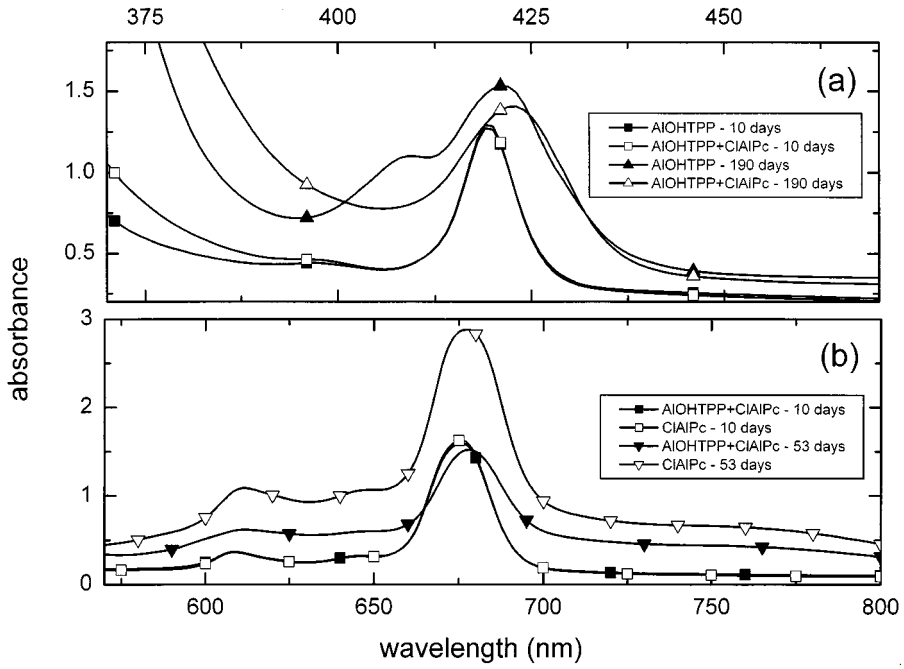

Fig. 21. Steady-state absorption spectra of ClAlPc and AlOHTPP, both separate and together, incorporated in SGD monoliths (route III) at different times after manufacture.

wavelength spectral region, which is dominated by the phthalocyanine absorption (Fig. 21b), if we compare the phthalocyanine spectrum in the presence and absence of porphyrin, it is noticeable in the sample with porphyrin, that there is a decrease and a red shift in the band close to 675 nm. The occurrence of a red shift in both spectral regions has been previously reported for porphyrin-phthalocyanine dimers [60], and here it is tempting to do the same. However, in that case the dimers were promoted by substitutions to the rings to provide a mutual attraction, although it also can be due to covalent linkage. The latter produces less drastic changes in the steady-state spectra, and in our case we would not expect a purely electrostatic promotion mechanism because the two species are non-ionic. However, the spectral trends of a red shift and decrease in absorption were also observed in solution, which indicate that a major feature of this system apparently is a porphyrin–phthalocyanine interaction.

Considering the fluorescence emission of the porphyrin in solution, on addition of phthalocyanine the spectra are essentially the superposition of the two. However on increasing phthalocyanine concentration there is a decrease in porphyrin emission, indicating a quenching process. An example of the emission at different times, using a SGD host are given in Fig. 22. This demonstrates a red shift with drying time, plus a decrease in the relative amount of phthalocyanine fluorescence. Time-resolved measurements were also performed, and examples are given in Table VII. Throughout for AlOHTPP there appear to be common lifetimes close to ~4 ns and ~7 ns in similar amounts in each of the media, although there is a small decrease in the lifetimes in a sample with phthalocyanine. Overall, the results show that there appears to be little interaction with the host matrix; moreover, if any mixed dimers are formed, they are non-fluorescent. We have not found significant evidence for dipole–dipole energy transfer and fitting the steady-state data to this model produced unrealistic values of R_o (over 100 Å). Also, unrealistic dynamic quenching rate constants were returned; thus the predominant intermolecular interactions appear to be those of dimer (or other aggregate) formation.

Assuming that the formation of non-fluorescent dimers is the major process we have endeavored to obtain approximate values for the dimerization constant, K_D:

$$K_D = \frac{[D]}{[P][Pc]} \tag{7}$$

Here $[D]$ is dimer concentration, $[P]$ is AlOHTPP concentration, and $[Pc]$ is ClAlPc concentration. This was done using the quenching data for both solution and SGD monolith represented in the inset in Fig. 22. The value for the solution data was found to be 5.7×10^4 M^{-1}, which, unsurprisingly, is about a thousand times smaller than that reported for those formed by electrostatic attraction [60]. In the titania host for low concentrations

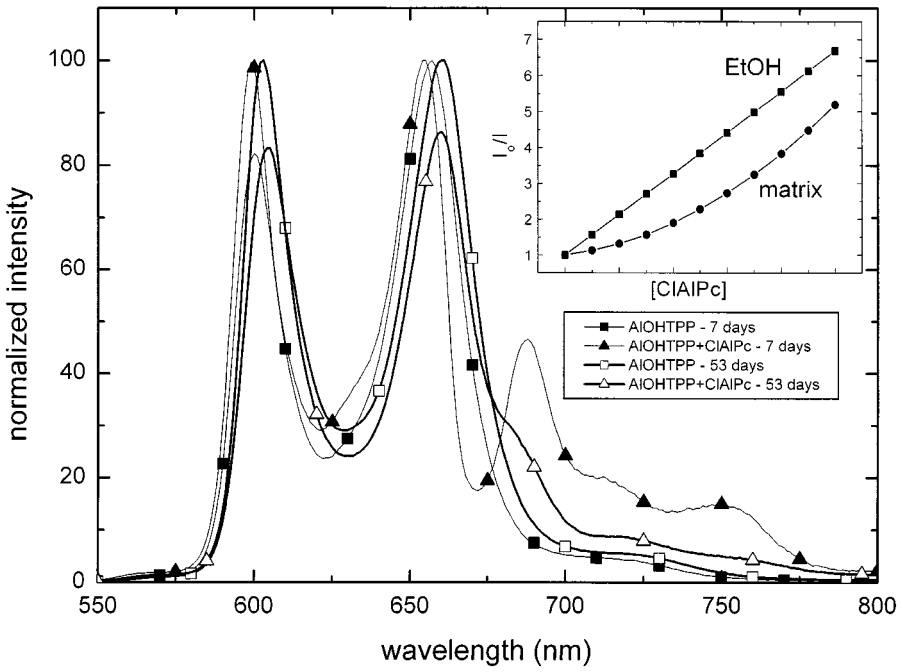

Fig. 22. Emission spectra of AlOHTPP and combined ClAlPc and AlOHTPP in a titania (route III with DMF) monolith. Inset change in AIOHTPP intensity with increasing CIAIPc concentration in both ethanol solution and in the SGD monolith.

the value is in the order of 2.9×10^4. For higher concentrations it is similar to the solution value. The lower value may relate to compartmentalization within the matrix pore structure. Overall with this system, although an energy transfer process cannot be entirely ruled out, it appears that the predominant quenching interaction involved the formation of non- (or negligibly) fluorescent dimers (or aggregates).

SUMMARY

In this paper we have described our recent work on the photophysics of dye-matrix systems, with both silica and titania matrices produced by sol-gel techniques. The role of solvents, either remaining from the sol-gel synthesis or deliberately added, determines to a large extent the fluorescence of the dyes we have studied. As a result, fluorescence tuning was examined because of its potential application in photonic devices. Dye-dye interactions have also been investigated for systems where dipole–dipole energy transfer by the Förster mechanism could be anticipated. The results obtained using Rhodamine 6G as a donor are indicative of geometrical confinement by the matrix pore structure, while those involving the aluminium porphyrin and phthalocyanine show that the presence of ground state aggregates compete with the Förster mechanism, although in the latter further studies are required.

REFERENCES

1. C. J. Brinker and G. W. Scherer (1990) *Sol-Gel Science: The Physics and Chemistry of Sol-Gel Processing*, Academic Press, New York.
2. R. Reisfeld (1990) Spectroscopy and applications of molecules in glasses. *J. Non-Cryst. Solids* **121**, 254–266.
3. D. Avnir (1995) Organic chemistry within ceramic matrices: doped sol-gel materials. *Acc. Chem. Res.* **28**, 328–334.
4. M. Casalboni, F. De Matteis, V. Ferone, P. Prosposito, R. Senesi, R. Pizzoferrato, A. Bianco, and A. De Mico (1998) DODCI molecules incorporated in sol-gel glasses: the interaction with the silica matrix. *Chem. Phys. Lett.* **291**, 167–172.
5. U. Narang, R. Wang, P. N. Prasad, and F. V. Bright (1994) Effects of aging on the dynamics of rhodamine 6G in tetramethyl orthosilicate derived sol-gels. *J. Phys. Chem.* **98**, 17–22.
6. L. M. Ilharco, A. M. Santos, M. J. Silva, J. M. G. Martinho (1995) Intramolecular pyrene excimer in probing the sol-gel process. *Langmuir* **11**, 2419–2422.
7. D. J. S. Birch and C. D. Geddes (2000) Sol-gel particle growth studied using fluorescence anisotropy: an alternative approach to scattering techniques. *Phys. Rev. E.* **62**, 2977–2980.
8. J. Karolin, C. D. Geddes, K. Wynne, D. J. S. Birch (2001) Nanoparticle metrology in sol-gels using multiphoton excited fluorescence. *Meas. Sci. Technol.* **13**, 21–27.
9. A. H. Boonstra, T. P. M. Meeuwsen, J. M. E. Baken, and G. V. A. Aben (1989) A 2-step silica sol-gel process investigated with static and dynamic light-scattering measurements. *J. Non-Cryst. Solids* **109**, 153–163.

10. A. L. Linsebigler, G. Lu, J. T. Yates Jr. (1995) Photocatalysis on TiO_2 surfaces—principles, mechanisms, and selected results. *Chem. Rev.* **95**, 735–758.
11. K. Kalyansundaram and M. Grätzel (1998) Applications of functionalized transition metal complexes in photonic and optoelectronic devices. *Coordination Chem. Rev.* **177**, 347–414.
12. C. Nasr, K. Vinodgopal, L. Fisher, S. Hotchandani, A. K. Chattopadhyay, and P. V. Kamat (1996) Environmental photochemistry on semiconductor surfaces. Visible light induced degradation of a texile diazo dye, naphthol blue black, on TiO_2 nanoparticles. *J. Phys. Chem.* **100**, 8436–8442.
13. K. Matsui and N. Usuki (1990) Excimer fluorescence of pyrene in sol-gel silica. *Bull. Chem. Soc. Jpn.* **63**, 3516–3520.
14. G. Hungerford, K. Suhling, and J. A. Ferreira (1999) Comparison of the fluorescence behaviour of rhodamine 6G in bulk and thin film tetraethylorthosilicate derived sol-gel matrices. *J. Photochem. Photobiol. A. Chem.* **129**, 71–80.
15. G. Hungerford and J. A. Ferreira (2001) The effect of the nature of retained solvent on the fluorescence of nile red incorporated in sol-gel derived matrices. *J. Luminesc* **93**, 155–165.
16. L. Hu, T. Yoko, H. Kozuka, and S. Sakka (1992) Effects of solvent on properties of sol-gel-derived TiO_2 coating films. *Thin Solid Films* **219**, 18–23.
17. M. Kallala, C. Sanchez, and B. Cabane (1993) Structures of inorganic polymers in sol-gel processes based on titanium dioxide. *Phys. Rev. E* **48**, 3692–3704.
18. D. McLoskey, D. J. S. Birch, A. Sanderson, K. Suhling, E. Welch, and P. J. Hicks (1996) Multiplexed single-photon counting. I. A time-correlated fluorescence lifetime camera. *Rev. Sci. Instrum.* **67**, 2228–2237.
19. K. Suhling, D. McLoskey and D. J. S. Birch (1996) Multiplexed single-photon counting. II. The statistical theory of time-correlated measurements. *Rev. Sci. Instrum.* **67**, 2238–2246.
20. K. Suhling, G. Hungerford, R. W. Airey, and B. L. Morgan (2001) A position sensitive photo event counting detector applied to the fluorescence imaging of dyes in sol-gel matrices. *Meas. Sci. Tech.* **12**, 131–141.
21. K. Suhling, R. W. Airey, and B. L. Morgan (1999) Optimisation of centroiding algorithms for photon event counting imaging. *Nucl. Instrum. Methods* **437**, 393–418.
22. K. Suhling, R. W. Airey, and B. L. Morgan (2002) Minimization of fixed pattern noise in photon event counting imaging. *Rev. Sci. Instrum.* **73**, 2917–2922.
23. J. I. Langford (1978) Rapid method for analysing breadths of diffraction and spectral-lines using voigt function. *J. Appl. Cryst.* **11**, 10–14.
24. T. Adachi and S. Sakka (1988) The role of N,N-dimethylformamide, a DCCA, in the formation of silica monoliths by sol-gel method. *J. Non-Cryst. Solids* **99**, 118–128.
25. I. Webman, J. Jortner, and M. H. Cohen (1977) Theory of optical and microwave properties of microscopically inhomogeneous materials. *Phys. Rev. B* **15**, 5712–5723.
26. G. Hungerford, M. I. C. Ferreira, M. R. Pereira, J. A. Ferreira, and A. F. Coelho (2000) Spectroscopic characterisation of phorphyrin-doped sol-gel-derived matrices. *J. Fluoresc.* **10**, 283–290.
27. T. M. R. Viseu, G. Hungerford, and M. I. C. Ferreira (2002) Optical and photophysical studies on porphyrin doped TiO_2 matrixes. *J. Phys. Chem. B* **106**, 1853–1861.
28. F. Abelès (1967) Chapter V in *Optics of Thin Films: Advanced Optical Techniques*, A. C. S. Van Heel (Ed.). North-Holland, Amsterdam.
29. A. R. Forouhi and I. Bloomer (1986) Optical dispersion-relations for amorphous-semiconductors and amorphous dielectrics. *Phys. Rev. B* **34**, 7018–7026.
30. K. K. Flora and J. D. Brennan (2001) Characterization of the microenvironments of PRODAN entrapped in tetraethyl orthosilicate derived glasses. *J. Phys. Chem. B* **105**, 12003–12010.
31. H. Soyez, M. Huang, B. Dunn, and J. I. Zink (1997) Probing the structural development of dip coated silica sol-gel thin films via fluorescent probe molecules. *Proc. SPIE* **3136**, 118–126.
32. D. C. Dong and M. A. Winnik (1984) The py scale of solvent polarities. *Can. J. Chem.* **62**, 2560–2565.
33. G. Hungerford, M. E. C. D. Real Oliveira, E. M. S. Castanheira, H. D. Burrows, and M. da G. Miguel (2002) Transitions in ternary surfactant/alkane/water microemulsions as viewed by fluorescence. *Prog. Colloid. Polymer. Sci.* In press.
34. J.-L. Habib Jiwan, E. Robert, and J.-Ph. Soumillion (1999) Sol-gel silicate thin films bearing attached pyrene fluorescing probes hidden from oxygen but still accessible to organic electron transfer quenchers. *J. Photochem. Photobiol. A. Chem.* **122**, 61–68.
35. P. Innocenzi, H. Kozuka, and T. Yoko (1996) Dimer-to-monomer transformation of rhodamine 6G in sol-gel silica films. *J. Non-Cryst. Solids* **201**, 26–36.
36. U. Narang, F. V. Bright, and P. N. Prasad (1993) Characterization of rhodamine 6G-doped thin sol-gel films. *Appl. Spectroscopy* **47**, 229–234.
37. M. N. Berberan-Santos, E. J. N. Pereira, and J. M. G. Martinho (1999) Chapter 3 in *Resonance Energy* Transfer, D. L. Andrews and A. A. Demidov (Eds.). Wiley, New York.
38. M. A. Victor and S. R. Croach (1995) Absorbance-corrected synchronous fluorescence with a fiber-optic-based fluorometer. *Appl. Spectroscopy* **49**, 1041–1047.
39. N. Tamai, T. Yamazaki, I. Yamazaki, A. Mizuma, and N. Mataga (1987) Excitation-energy transfer between dye molecules adsorbed on a vesicle surface. *J. Phys. Chem.* **91**, 3503–3508.
40. J. R. Lakowicz (1983) *The Principles of Fluorescence Spectroscopy*, Plenum Press, New York.
41. E. Stathatos, P. Lianos, and C. Krontiras (2001) Dye-sensitized photoelectrochemical cell using a nanocomposite SiO_2/poly(ethylene glycol) thin film as electrolyte support. Characterisation by time-resolved luminescence and conductivity measurements. *J. Phys. Chem. B* **105**, 3486–3492.
42. M. J. M. F. Monteiro Capelo (1996) *Espectroscopia de absorção e emissão da Rodamina 6G adsorvida em TiO_2*. Masters Thesis, Universidade do Minho, Braga, Portugal.
43. J. M. Drake, M. L. Lesiecki, and D. M. Cameron (1985) Photophysics and cis-trans isomerization of DCM. *Chem. Phys. Lett.* **113**, 530–534.
44. M. Meyer, J. C. Mialocq, and B. Perly (1990) Photoinduced intramolecular charge transfer and cis-trans isomerization of the DCM styrene dye. Picosecond and nanosecond laser spectroscopy, high performance liquid chromatography and nuclear magnetic resonance studies. *J. Phys. Chem.* **94**, 98–104.
45. P. R. Hammond (1979) Laser dye DCM, its spectral properties, synthesis and comparison with other dyes in the red. *Opt. Commun.* **29**, 331–333.
46. L. Hu and Z. Jiang (1997) Laser performance in dye molecules doped xerogels. *Proc. SPIE* **3136**, 94–101.
47. A. Dubois, M. Canva, A. Brun, F. Chaput, and J.-P. Boilot (1996) Photostability of dye molecules trapped in solid matrices. *Appl. Optics* **35**, 3193–3199.
48. G. Hungerford and J. A. Ferreira. Submitted for publication.
49. B. Strehmel and W. Rettig (1996) Photophysical properties of fluorescence probes I. dialkylamino stilbazolium dyes. *J. Biomed. Opt.* **1**, 98–109.
50. G. Hungerford, E. M. S. Castanheira, M. E. C. D. Real Oliveira, M. da G. Miguel, H. D. Burrows (2002) Monitoring ternary systems of $C_{12}E_5$/water/tetradecane via the fluorescence of solvatochromic probes. *J. Phys. Chem. B.* **106**, 4061–4069.
51. M. Meyer and J. C. Mialocq (1987) Ground state and singlet excited state of laser dye DCM: dipole moments and solvent induced spectral shifts. *Opt. Commun.* **64**, 264–268.
52. A. K. Dutta, K. Kamada, and K. Ohta (1996) Spectroscopic studies of nile red in organic solvents and polymers. *J. Photochem. Photobiol. A. Chem.* **93**, 57–64.

53. D. L. Sackett, J. R. Knutson, and J. Wolff (1990) Hydrophobic surfaces of tubulin probed by time-resolved and steady-state fluorescence of nile red. *J. Biol. Chem.* **265**, 14899–14906.
54. M. M. G. Krishna (1999) Excited state kinetics of the hydrophobic probe nile red in membranes and micelles. *J. Phys. Chem. A.* **103**, 3589–3595.
55. M. Ochsner (1997) Photophysical and photobiological processes in the photodynamic therapy of tumours. *J. Photochem. Photobiol. B. Biol.* **39**, 1–18.
56. D. Delamarre, R. Méallet, C. Bied-Charreton, and R. B. Pansu (1999) Heavy metal ions detection in solution, in sol-gel and with grafted porphrin monolayers. *J. Photochem. Photobiol. A. Chem.* **124**, 23–28.
57. V. S. Chirvony, A. van Hoek, V. A. Galievsky, I. V. Sazanovich, T. J. Schaafsma, and D. Holten (2000) Comparative study of the photophysical properties of nonplanar tetraphenylporphyrin and octaethylporphyrin diacids. *J. Phys. Chem. B.* **104**, 9909–9917.
58. J. Kossanyi and D. Chahraoui (2000) Electron transfer reaction and demetalation of phthalocyanines. *Int. J. Photoenergy* **2**, 9–15.
59. P. D. Fuqua, B. Dunn, and J. I. Zink (1998) Optical properties and dimer formation in copper phthalocyanine-doped sol-gel matrices. *J. Sol-Gel Sci. Technol.* **11**, 241–250.
60. T. H. Tran-Thi, J. F. Lipskier, D. Houde, C. Pépin, E. Keszei, and J. P. Jay-Gerin (1992) Subpicosecond excitation of strongly coupled porphyrin-phthalocyanine mixed dimers. *J. Chem. Soc. Faraday Trans.* **88**, 2129–2137.